(Received 11 July 2025, Accepted 22 October 2025, Scheduled 3 November 2025)

Selective Signal Transmission and Crosstalk Suppression Based on Double-Layer RFID Tags

Peiying Lin[1, 2], Jiangtao Huangfu[3], Xixi Wang[4], Dana Oprisan[4], and Yanbin Yang[1, *]

[1] *Artificial Intelligence College, Sichuan Tourism University, Chengdu 610230, Sichuan, China*
[2] *School of Electrical and Information Engineering, Jiangsu University of Science and Technology, Suzhou 215600, Jiangsu, China*
[3] *Laboratory of Applied Research on Electromagnetics, Zhejiang University, Hangzhou 310027, Zhejiang, China*
[4] *EPF Engineering College, 2 rue Fernand Sastre, Rosières-près-Troyes 10430, France*

ABSTRACT: This paper presents a passive, structure-based approach for selective signal transmission and crosstalk suppression in dense radio frequency identification (RFID) tag environments. The proposed method employs a mechanically reconfigurable double-layer tag design based on the mirror-antenna principle, which enables dynamic switching between transmission and shielding modes by adjusting the interlayer spacing. Simulation results demonstrate pronounced differences in the reflection characteristics and radiation intensity of the tag under the two operating modes at 915 MHz. Experimental validation further confirms the effectiveness of the system in mitigating interference and ensuring reliable tag identification in multi-tag scenarios. The design is compact, energy-efficient, and cost-effective, supporting scalable applications in smart retail and automated inventory management.

1. INTRODUCTION

With the rapid advancement of the Internet of Things (IoT), RFID has emerged as a widely adopted non-contact and efficient automatic identification technology. It has found extensive applications in smart retail, warehouse logistics, supply chain management, and other domains [1–4]. Compared with camera-based recognition systems, which are highly sensitive to ambient lighting conditions and prone to errors under low light, reflections, or occlusions, RFID systems offer significant advantages. Vision-based systems also suffer from high computational complexity, privacy concerns, and deployment challenges [5]. Similarly, infrared and other sensing technologies often rely on strict structural conditions and are susceptible to false triggers or missed detections, limiting their flexibility and reliability in dynamic environments [6]. In contrast to traditional barcode systems, RFID enables batch reading, does not require line-of-sight, and offers fast data access, greatly enhancing the automation and intelligence of logistics and retail operations [7]. As product displays become increasingly digitized and interactive, the deployment of multiple tags in close proximity has become commonplace [8]. However, dense tag environments pose serious challenges for conventional RFID systems, such as signal crosstalk, redundant readings, sluggish response, and data ambiguity [9]. Active tags integrate power and onboard processing, enabling autonomous communication, whereas passive tags lack coordination capabilities [10]. In practical applications, the use of clustered RFID tags is limited by cost, with passive tags being predominantly adopted [11]. When multiple passive tags respond simultaneously, collisions inevitably occur on the shared channel [12].

The predominant line of work in RFID anti-collision has relied on algorithmic solutions at the reader side. Classical protocols such as ALOHA [13] and tree-based algorithms [14] employ time- or code-division schemes to reduce response collisions, but they suffer from limited throughput and increased latency under dense deployments [15]. Machine learning has recently been introduced, e.g., a classifier chain — AdaBoost (CC-AdaBoost) model achieving about 85% classification accuracy [16], yet scalability remains a challenge. Other approaches attempt to enhance robustness by jointly controlling the amplitude and phase of passive RFID tags [17–19], thereby compensating for tag position variations and multipath propagation. In multi-tag localization scenarios, the combination of non-metric multidimensional scaling (NMDS) with fingerprinting-based methods has shown potential for cooperative indoor positioning [20]. In chipless RFID, signal separation methods such as time-difference-of-arrival (TDoA) estimation and time-frequency analysis via the short-time matrix pencil method (STMPM) [21] have been applied to distinguish multiple tags. When integrated with one-dimensional convolutional neural network (1-DCNN), features extracted by STMPM, such as complex natural resonances (CNRs) and natural frequencies, can be used for improved classification [22]. Despite these advances, algorithmic solutions generally incur protocol complexity and computational overhead, which scale poorly as tag density increases [23].

From a hardware perspective, optimizing antenna design to enable differential responses has gained attention. Multi-polarized antennas can distinguish signals based on polariza-

* Corresponding author: Yanbin Yang (sinhei@163.com).

tion orientation, reducing interference between tags [24, 25]. By optimizing the electric field distribution of a reader antenna [26], efficient and low-interference tag identification in near-field applications can be achieved. Frequency agility techniques have also been proposed to switch tags across different frequency bands, thereby mitigating co-channel interference, including the use of tunable multi-band RFID antennas [27]. In addition, multi-port antennas can dynamically switch between operating modes such as near-field and far-field modes to suit various application scenarios [28]. Antenna array technologies further leverage spatial filtering and beamforming to enhance target tag signals while suppressing interference from non-target tags [29]. Beyond protocol-level solutions, antenna optimization combined with signal processing offers another pathway for anti-collision. For instance, space-division multiple access (SDMA) with beam-switching antennas can separate tag IDs [30], while blind source separation (BSS) with diode-controlled beam reconfiguration and independent component analysis (ICA) enables the separation of adjacent tags without time-difference estimation [31]. Additionally, the widely linear minimum-mean-square-error (WLMMSE) method [32] efficiently separates overlapping tag responses within a single time slot and can be integrated into multi-antenna systems to improve throughput. These hardware-oriented approaches complement protocol-level schemes by directly improving the physical-layer separability of tag responses, though their reliance on complex circuitry and active control may still hinder large-scale, low-cost deployments.

Passive RFID tags generally lack spatial selectivity, which causes crosstalk and misreadings in dense deployments [33]. To overcome this, structural design enabling selective responses has been investigated [34]. For example, multilayer plasmonic covers can produce comb-like scattering responses for optical tagging [35], but their applicability to the radio frequency (RF) band and dense multi-tag scenarios remains largely unexplored. Metallic edges and curved scatterers [36] offer a novel strategy for selective responses, with promising potential in multi-tag system design. Dynamic control methods provide another line of exploration, such as epidermal passive RFID strain sensors based on mechanical compression [37], RF micro-electromechanical system (MEMS) structures that enable tunable antenna parameters [38], and integrated switch-based sensing schemes [39]. These solutions demonstrate the feasibility of physically controlling tag states with advantages of zero power consumption and structural simplicity [40], but challenges remain in terms of complexity, manufacturing scalability, and robustness under large-scale multi-tag deployments [41, 42].

In this work, a selective signal transmission and shielding method is proposed based on a double-layer RFID tag structure. By mechanically adjusting the interlayer spacing, the tag can switch between transmission and shielded modes, thereby suppressing crosstalk and improving signal quality in dense environments. The design operates without external power and achieves mode switching purely through structural deformation, offering clear functional response and ease of integration. The remainder of this paper is organized as follows:

- Section 2 outlines the architecture of the proposed selective signal transmission system and details its working principle based on the mirror antenna effect, including the structural configuration of the double-layer RFID tag.
- Section 3 evaluates the electromagnetic behavior of the tag through full-wave simulation, focusing on its transmission and radiation characteristics in different operational modes.
- Section 4 details the system implementation and experimental validation under both single-tag and multi-tag conditions.
- Section 5 summarizes the findings and discusses the potential applications of the proposed design in smart retail and IoT scenarios.

2. SYSTEM ARCHITECTURE AND PRINCIPLE

2.1. System Architecture

The proposed selective signal transmission system is composed of four main components: double-layer RFID tags, a directional reader antenna, an RFID reader, and a control terminal, as illustrated in Fig. 1. The double-layer RFID tag integrates an RFID chip and a double-layer antenna arranged in a vertically stacked configuration. By mechanically adjusting the vertical spacing between the two antenna layers, the tag can dynamically switch between signal transmission and signal shielding modes, enabling selective responsiveness to the reader's interrogation signals.

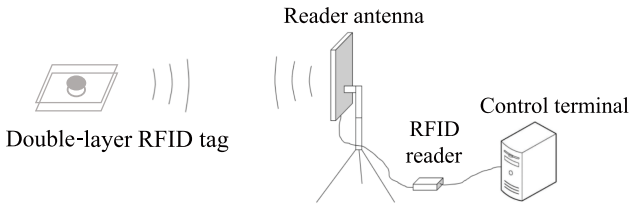

FIGURE 1. Selective signal transmission system.

The reader antenna is directional and operates under command from the control terminal, transmitting and receiving signals within a specified angle and power range. The RFID reader generates interrogation signals and receives responses from the tags, enabling data exchange and identification. Acting as the system's control center, the terminal coordinates signal processing, environmental monitoring, and dynamic adjustment of reader parameters. It also integrates response data from multiple tags to effectively suppress interference and extract relevant information. This architecture leverages the synergy of hardware and software to ensure reliable and efficient operation in complex, multi-tag environments.

2.2. Principle

The double-layer RFID tag comprises an RFID chip and a double-layer antenna structure, where the upper layer functions

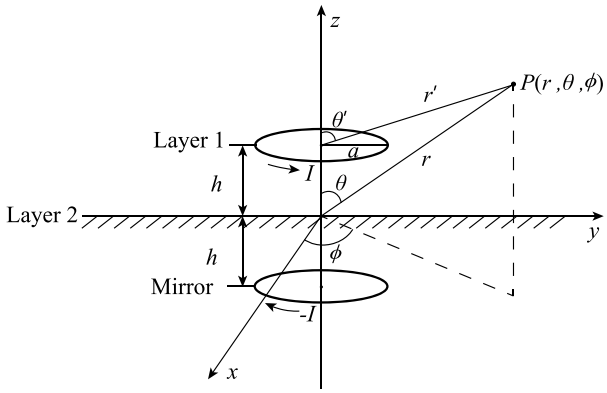

FIGURE 2. Mirror antenna principle. Layer 1: Signal transceiving layer. Layer 2: Signal shielding layer.

as the signal transceiving element and the lower layer serves as a signal shielding plane. The key feature lies in the use of mechanical deformation to switch between operating modes, governed by the principle of image antenna theory [43]. The shielding layer, made of a conductive material, induces mirror currents in response to the electromagnetic field generated by the transceiving layer placed above it. According to the mirror antenna theory, the radiation field produced by these image currents can be equivalently represented by a virtual antenna that mirrors the original one across the conductive plane. The resulting configuration behaves as an equivalent two-element antenna array, as illustrated in Fig. 2.

Let the vertical spacing between the two layers be h, and therefore the image of the transceiving layer is also located at a distance h below the shielding layer. The total radiation field at point P, denoted by $\overline{E}_p$, is the superposition of the direct radiation field $\overline{E}_{ant}$ and the mirrored radiation field $\overline{E}_{mir}$:

$$\overline{E}_p = \overline{E}_{ant} + \overline{E}_{mir} \tag{1}$$

In the case of a horizontal two-element antenna array with equal amplitude and opposite phase, if the transceiving layer is modeled as an electrically small loop antenna with radius h, $\overline{E}_{ant}$ can be expressed by Equation (2), where I denotes the current along the loop, J_1 the first-order Bessel function, and k the phase constant. The normalized overall radiation pattern [44] of the double-layer antenna is given by Equation (3). By adjusting the interlayer distance h, the spatial phase difference between the two layers can be modified, thereby modulating the overall antenna gain pattern and radiation intensity.

$$\overline{E}_{ant} = \frac{60\pi kIa}{2r'} J_1(ka\sin\theta') \tag{2}$$

$$f(\theta,\phi) = \sin\theta\,|\sin(kh\cos\theta)| \tag{3}$$

2.3. Structural Parameters

According to the aforementioned principle, the vertical distance h between the two layers determines the operating mode of the RFID tag — either signal transmission or signal shielding. When the tag operates in the transmission mode, the spacing h is set to 3 mm, enabling effective communication with the RFID reader. In the shielding mode, the two layers are closely attached with a vertical gap less than 0.2 mm, significantly attenuating the signal strength and preventing the tag from being recognized by the reader. The transition between the two modes is mechanically controlled by changing the interlayer distance. To achieve this, a deformable non-metallic spacer, such as a spring or foam, is inserted between the layers. External pressure applied to the antenna surface compresses the structure, altering h and thereby switching the tag's functional mode. The antenna design, as illustrated in Fig. 3, features a double-layered concentric ring configuration with a radius of 6 mm, where each individual layer has a thickness of 0.1 mm. The signal transceiving layer employs a flexible PET film as the substrate, with a thickness of 100 µm and a dielectric constant of 3.2. Both layers are fixed using acrylic sheets. The detailed structural parameters are listed in Table 1. By tuning the geometry and dimensions of the antenna, impedance matching with the RFID chip is optimized to improve energy transfer efficiency near the target frequency of 915 MHz.

TABLE 1. Double-layer RFID tag antenna parameter dimensions.

Parameters	Dimensions (mm)	Parameters	Dimensions (mm)
d_0	12.00	l_1	4.10
d_1	0.64	l_2	0.45
d_2	0.55	l_3	0.74
d_3	0.40	l_4	0.25
a_s	5.00	w_0	1.00
r_1	0.40	w_1	0.50
r_2	0.80	w_2	0.10
l_s	50.00	θ_1	40°

3. SIMULATION AND ANALYSIS

To assess the electromagnetic characteristics and dynamic switching capability of the proposed double-layer RFID tag, full-wave simulations were performed using Computer Simulation Technology (CST) Microwave Studio. The analysis focused on verifying the tag's communication efficiency in the signal transmission mode and its interference suppression performance in the signal shielding mode. Simulation results, illustrated in Figs. 4–5, reveal distinct differences in signal propagation and radiation strength between the two modes.

The simulated reflection coefficient S_{11} curves for the double-layer RFID tag antenna under various values of h are presented in Fig. 4, over a frequency range of 0–2 GHz. As depicted, the optimal matching occurs at $h = 3$ mm, where a minimum S_{11} of -40.96 dB is achieved at 915 MHz. This deep resonance indicates minimal energy reflection and, consequently, high signal transmission efficiency, which arises from a conjugate match between the antenna's input impedance and the RFID chip impedance $Z_{chip} = 3 - j114\,\Omega$ at 915 MHz. While the antenna remains functional around 915 MHz for $h > 3$ mm, a higher external mechanical pressure is required for mode switching. Therefore, $h = 3$ mm is selected as the

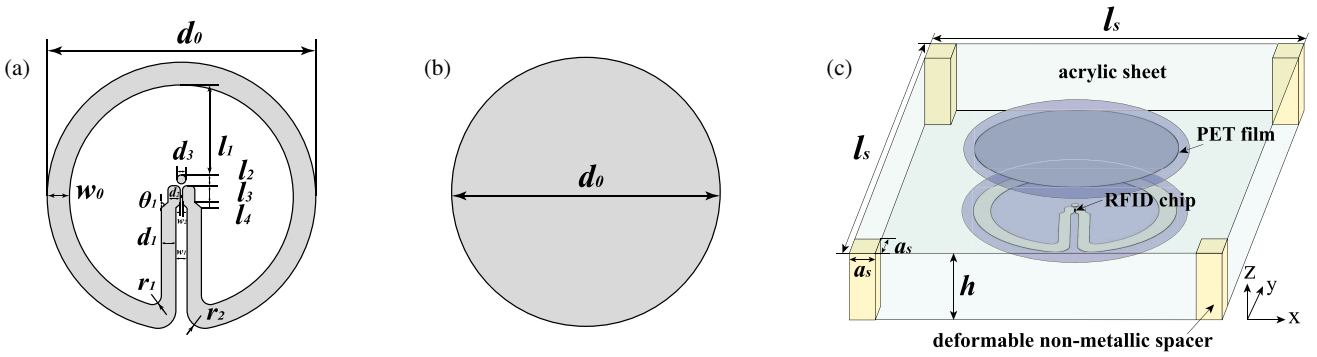

FIGURE 3. Structure of the proposed double-layer RFID tag antenna: (a) Signal transceiving layer, (b) signal shielding layer, and (c) vertically stacked double-layer configuration. From top to bottom, the layers are arranged as: acrylic sheet-PET film-shielding layer-transceiving layer-PET film-acrylic sheet.

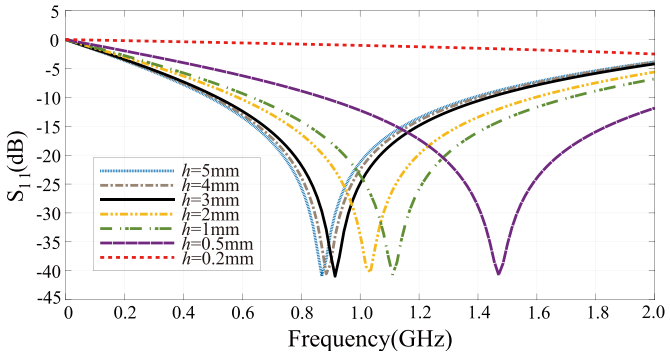

FIGURE 4. Simulated curves of reflection coefficient S_{11} of double-layer RFID tag antenna.

transmission mode. In contrast, as h decreases, the resonant frequency exhibits a noticeable shift. When h is reduced to 0.2 mm or less, the matching performance deteriorates significantly across the 0–2 GHz band, with S_{11} of -0.92 dB at 915 MHz. This high reflection coefficient signifies that the antenna is in shielding mode, leading to severely degraded communication between the tag and the reader.

Figure 5 illustrates the simulated radiation patterns of the double-layer RFID tag antenna in both operational modes. A pronounced contrast is observed, with a radiation intensity difference of 12.47 dB between the modes, demonstrating the tag's effective radiation control mechanism. Specifically, the transmission mode achieves a maximum gain of 4.55 dBi, indicative of strong directionality and efficient radiation for stable reader communication. Conversely, the shielding mode exhibits a significantly reduced upward gain of -7.92 dBi, confirming the effective suppression of electromagnetic radiation. These results collectively verify that the proposed design enables effective radiation control through structural deformation, offering robust spatial selectivity.

4. EXPERIMENTAL VALIDATION

To comprehensively evaluate the feasibility and practical effectiveness of the proposed double-layer RFID tag in real-world applications, a complete selective signal transmission testing system was constructed, as depicted in Fig. 6. The system comprises four main components: a custom-fabricated double-layer RFID tag, an Impinj E310 UHF RFID reader, a ceramic directional antenna, and an external USB communication module that bridges data exchange between the reader and control terminal. The operational read range of the system is characterized by a maximum distance of 2 meters. This limitation is imposed by the constraints of the reader's transmitting power of 16 dBm and the antenna's directivity, which features a gain of 4 dBi with a read angle of 120°. Neglecting transmission losses, the maximum Equivalent Isotropically Radiated Power (EIRP) of the system was calculated to be 20 dBm.

The double-layer RFID tags were prototyped based on the simulation design using aluminum for the antenna elements and integrated with NXP UCODE 9 chips, as shown in Fig. 7. The tag's structural innovation lies in its mechanically tunable interlayer spacing: the two antenna layers — namely, signal transceiving layer and shielding layer — are connected via a compressible foam spacer. This passive mechanical design enables physical deformation under external pressure, dynamically adjusting the vertical distance h between the layers. When pressure is applied to the tag surface, the layers come into close contact ($h < 0.2$ mm), effectively suppressing electromagnetic radiation and switching the tag to shielding mode. Conversely, in the absence of pressure, the vertical distance h remains around 3 mm, allowing efficient signal transmission.

Experimental validation was conducted in two primary phases:

- Single-tag mode switching test — to measure the tag's responsiveness and signal strength under transmission and shielding modes.
- Multi-tag interference test — to assess the system's ability to selectively identify active tags in densely populated tag environments and to evaluate its robustness against cross-reading or signal collision.

This testing framework aims to validate not only the electromagnetic behavior predicted by simulation but also the mechanical switching performance and application viability of the proposed design in dynamic, real-world retail environments.

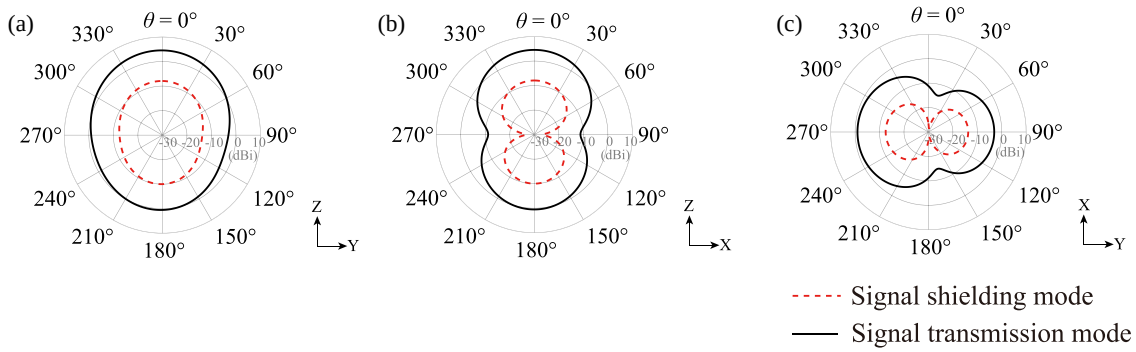

FIGURE 5. Simulated radiation patterns of the double-layer RFID tag antenna in different modes: (a) yz plane, (b) xz plane, (c) xy plane.

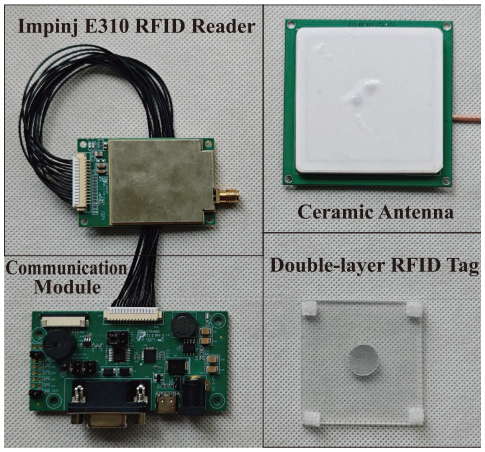

FIGURE 6. Photograph of RFID selective signal transmission test system.

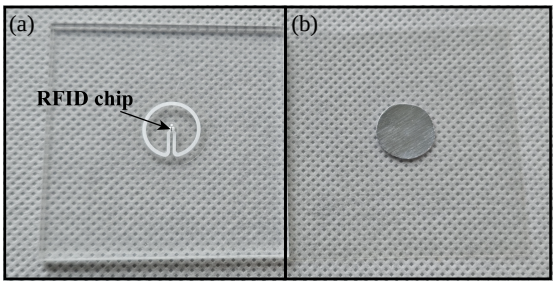

FIGURE 7. Photographs of the two separate layers of the proposed RFID tag: (a) Signal transceiving layer. (b) Signal shielding layer, transceiver layer below shielding layer.

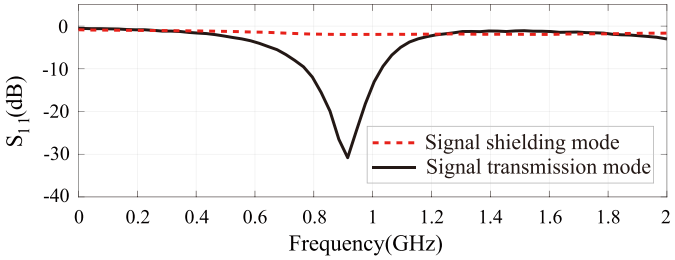

FIGURE 8. Measured curves of reflection coefficient S_{11} of double-layer RFID tag antenna.

4.1. Single-Tag Mode Switching Test

To evaluate the mode-switching capability of the proposed double-layer RFID tag under controlled conditions, a single-tag experiment was conducted, focusing on its performance in both the signal transmission and shielding modes. This section presents results of the reflection coefficient and communication link quality. First, the reflection coefficient was measured for both modes. As shown in Fig. 8, the antenna in the transmission mode exhibits optimal impedance matching near 915 MHz, with a minimum S_{11} of -30.81 dB, indicating low energy loss and high transmission efficiency. In contrast, the matching performance deteriorates markedly in the shielding mode across the entire band, showing an S_{11} of only -2.11 dB at 915 MHz, which implies severe signal reflection and ineffective communication.

Second, the communication quality was assessed via the Received Signal Strength Indicator (RSSI) with a fixed tag-reader distance of 1.5 meters. When the tag was in its transmission mode — that is, when the vertical gap h was maintained at 3 mm without any external pressure — the average RSSI was recorded at -48 dBm, indicating strong signal reception and stable communication with the reader. This confirms the tag's effectiveness in normal operation when uncompressed. Conversely, when the tag was subjected to external mechanical pressure, causing the foam spacer between the antenna layers to compress and reduce the vertical gap h to below 0.2 mm, the tag entered the shielding mode. At this point, the measured average RSSI dropped below -70 dBm, with the signal strength falling below the reader's decoding threshold, insufficient to support normal communication. This demonstrates the system's capability to block undesired communication through purely mechanical means, without requiring any electrical or software-based control.

To validate the repeatability and mechanical robustness of the switching mechanism, the same tag underwent 50 consecutive switching cycles between transmission and shielding modes. During each cycle, the tag was alternately compressed and released to simulate typical interactions. Throughout these tests, the system maintained a 100% successful recognition rate in the transmission mode and complete shielding in the inactive state. Moreover, the average response time for switching between modes was measured to be less than one second, con-

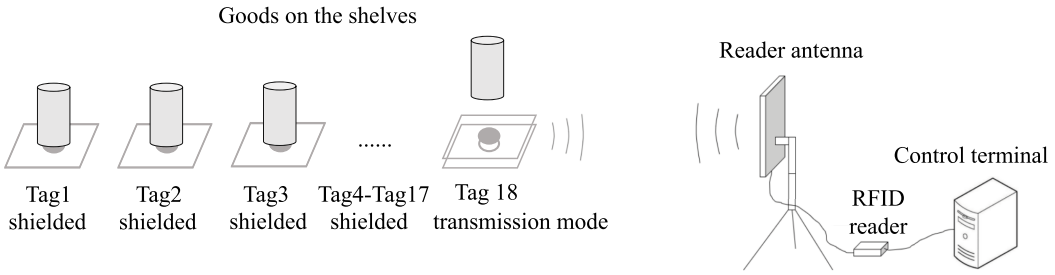

FIGURE 9. Multi-tag commodity display system with selective signal transmission.

TABLE 2. Test results of the multi-tag system.

RSSI (dbm) Read rate (%)	Tag 1	Tag 2	Tag 3	Tag 4	Tag 5	Tag 6	Tag 7	Tag 8	Tag 9	Tag 10	Tag 11	Tag 12	Tag 13	Tag 14	Tag 15	Tag 16	Tag 17	Tag 18
Test 1	-46 99.9	N/A	N/A	N/A	N/A	N/A	N/A	N/A	N/A	N/A	N/A	N/A	N/A	N/A	N/A	N/A	N/A	N/A
Test 2	N/A	-47 99.8	N/A	N/A	N/A	N/A	N/A	N/A	N/A	N/A	N/A	N/A	N/A	N/A	N/A	N/A	N/A	N/A
Test 3	N/A	N/A	-49 98.8	N/A	N/A	N/A	N/A	N/A	N/A	N/A	N/A	N/A	N/A	N/A	N/A	N/A	N/A	N/A
Test 4	N/A	N/A	N/A	-46 99.7	N/A	N/A	N/A	N/A	N/A	N/A	N/A	N/A	N/A	N/A	N/A	N/A	N/A	N/A
Test 5	N/A	N/A	N/A	N/A	-47 99.6	N/A	N/A	N/A	N/A	N/A	N/A	N/A	N/A	N/A	N/A	N/A	N/A	N/A
Test 6	N/A	N/A	N/A	N/A	N/A	-48 99.5	N/A	N/A	N/A	N/A	N/A	N/A	N/A	N/A	N/A	N/A	N/A	N/A
Test 7	N/A	N/A	N/A	N/A	N/A	N/A	-48 99.8	N/A	N/A	N/A	N/A	N/A	N/A	N/A	N/A	N/A	N/A	N/A
Test 8	N/A	N/A	N/A	N/A	N/A	N/A	N/A	-46 99.5	N/A	N/A	N/A	N/A	N/A	N/A	N/A	N/A	N/A	N/A
Test 9	N/A	N/A	N/A	N/A	N/A	N/A	N/A	N/A	-49 99.6	N/A	N/A	N/A	N/A	N/A	N/A	N/A	N/A	N/A
Test 10	N/A	N/A	N/A	N/A	N/A	N/A	N/A	N/A	N/A	-47 98.9	N/A	N/A	N/A	N/A	N/A	N/A	N/A	N/A
Test 11	N/A	N/A	N/A	N/A	N/A	N/A	N/A	N/A	N/A	N/A	-49 98.8	N/A	N/A	N/A	N/A	N/A	N/A	N/A
Test 12	N/A	N/A	N/A	N/A	N/A	N/A	N/A	N/A	N/A	N/A	N/A	-50 99.7	N/A	N/A	N/A	N/A	N/A	N/A
Test 13	N/A	N/A	N/A	N/A	N/A	N/A	N/A	N/A	N/A	N/A	N/A	N/A	-47 99.6	N/A	N/A	N/A	N/A	N/A
Test 14	N/A	N/A	N/A	N/A	N/A	N/A	N/A	N/A	N/A	N/A	N/A	N/A	N/A	-48 99.5	N/A	N/A	N/A	N/A
Test 15	N/A	N/A	N/A	N/A	N/A	N/A	N/A	N/A	N/A	N/A	N/A	N/A	N/A	N/A	-47 99.8	N/A	N/A	N/A
Test 16	N/A	N/A	N/A	N/A	N/A	N/A	N/A	N/A	N/A	N/A	N/A	N/A	N/A	N/A	N/A	-46 99.9	N/A	N/A
Test 17	N/A	N/A	N/A	N/A	N/A	N/A	N/A	N/A	N/A	N/A	N/A	N/A	N/A	N/A	N/A	N/A	-49 99.7	N/A
Test 18	N/A	N/A	N/A	N/A	N/A	N/A	N/A	N/A	N/A	N/A	N/A	N/A	N/A	N/A	N/A	N/A	N/A	-47 99.7

firming the system's suitability for real-time interactive applications.

These results highlight the reliability, stability, and responsiveness of the proposed double-layer structure. The purely passive, mechanically triggered switching mechanism not only simplifies the design but also ensures long-term operability without performance degradation, making it especially suitable for dense deployment in retail, warehousing, and other IoT-driven environments.

4.2. Multi-Tag Interference Test

In practical applications such as product displays, multiple RFID tags are often deployed in close proximity. To simulate such scenarios, a multi-tag demonstration system was constructed using 18 double-layer RFID tags, each separated by 0.8 cm and assigned a unique ID. Each tag was positioned beneath a designated product location. When a product rests on a tag, it applies pressure that activates the shielding mode, preventing the tag from communicating. When a product is picked up by a customer, the pressure is removed, shifting the tag to

TABLE 3. Comparison between the proposed work and existing multi-tag identification methods.

Ref.	Method & Hardware	Number of tags	Tag separation distance (cm)	Dimension (λ^2)	Multi-tag identification accuracy	Read range (m)
[16]	CC-Adaboost	7	1	0.40×0.40	85%	0.6
[20]	NMDS & 16 reference tags	30	200	N/A	Positioning error ≤ 1.6 m (80%)	8.0
[21]	STMPM & CNRs	2	20	0.44×0.44	Positioning error ≤ 0.01 m	0.5
[22]	1-DCNN & STMPM	8	3	0.40×0.40	100%	0.2
[31]	BSS & Pattern reconfigurable antenna	4	0.6	0.50×0.50	100%	0.1
Proposed	Double-layer RFID tags	18	0.8	0.04×0.04	100%	1.5

the transmission mode and triggering communication with the reader. Products under test are required to have a mass exceeding 50 g to provide adequate pressure for maintaining the tags in their shielding mode. Fig. 9 illustrates a snapshot of the test scenario: Tags 1 to 17 are in the shielding mode due to products resting on them, thus remaining inactive to the reader. Tag 18, corresponding to the lifted product, switches to the transmission mode and successfully establishes communication with the terminal, triggering the display of the product information. Once the product is returned, Tag 18 reverts to the shielding mode, and communication is interrupted accordingly.

Table 2 summarizes the multi-round system test results, with Test 1–Test 18 corresponding to Tag 1–Tag 18 being activated for communication. "N/A" indicates that the signal strength falls below the decodable threshold of -70 dBm, at which point the tag is in shielding mode. When the average RSSI value and read success rate are recorded, the tag is in transmission mode. Fig. 9 corresponds to Test 18, where Tag 18 is activated. To evaluate long-term stability, the system was continuously operated for 60 minutes, with each tag being triggered over 300 times. The multi-tag identification accuracy remained at 100%, with no false activations or data confusion. The test confirms that only the tag under the lifted product enters communication, avoiding multi-tag responses and preventing signal collision. This "lift-to-display, place-to-hide" mechanism enables an intuitive and interactive information display without requiring any power supply or active component in the product itself. The system leverages mechanical deformation of the tag to determine communication status, simplifying system design while enhancing scalability and deployment convenience.

The overall results demonstrate that the selective signal transmission system based on the proposed double-layer RFID tag significantly improves tag identification accuracy and effectively reduces cross-reading occurrences. The mechanism enabling precise detection of product pick-and-place actions through the double-layer tag structure can be widely applied in retail terminals, unmanned stores, and similar scenarios. It enhances the precision and interactivity of product display information, addresses the issues of indiscriminate tag responses in conventional RFID shelving that lead to cross-reading and misreading, and thereby reduces the risk of incorrect information identification.

A comparative analysis of the proposed work and existing multi-tag identification schemes is presented in Table 3, focusing on identification accuracy in dense tag scenarios. Previous approaches typically face a fundamental trade-off: high identification accuracy comes at the expense of limited reading range and a constrained number of identifiable tags. The proposed method, in contrast, mitigates this trade-off through its mechanically-controlled mode switching. This mechanism ensures high accuracy while maintaining a long reading range, thereby supporting the large-scale deployment of small-sized, passive tags. Another significant advantage lies in its operational simplicity and the ease of hardware implementation. The primary limitations, however, include potential mechanical fatigue over time and incompatibility with very lightweight items such as feathers.

5. CONCLUSION

This work proposes a selective signal transmission and shielding method based on a mechanically reconfigurable double-layer RFID tag, aiming to address challenges such as crosstalk and misidentification in dense deployments. A complete signal control and product display system is developed around this design. Simulation results verify that the system exhibits excellent mode-switching capability and significant radiation control performance in the UHF RFID band. Experimental results further confirm the tag's ability to switch modes reliably in both single- and multi-tag scenarios, enabling the accurate detection of object interaction events. The double-layer structure, which enables passive switching through mechanical deformation, features low cost, structural simplicity, and ease of deployment. It effectively reduces cross-tag interference and improves identification precision, making it highly suitable for smart shelves, unmanned retail systems, and fine-grained warehouse management. Overall, this solution provides a practical and scalable approach to selective RFID communication in IoT applications, offering substantial value for the large-scale deployment of intelligent identification systems.

ACKNOWLEDGEMENT

This study is supported by Chengdu Longquanyi Science and Technology Program 2024LQYF0019.

REFERENCES

[1] Tebaldi, L., D. Reverberi, G. Romagnoli, E. Bottani, and A. Rizzi, "RFID technology in retail 4.0: State-of-the-art in the fast-moving consumer goods field," *International Journal of RF Technologies*, Vol. 13, No. 2, 105–133, 2023.

[2] Wickramasinghe, S., J. Jayasinghe, G. N. A. Mohammed, M. Senadeera, and M. Kanagasabai, "A compact energy harvesting RFID tag for smart traffic law enforcement systems," *Progress In Electromagnetics Research C*, Vol. 135, 181–193, 2023.

[3] Khan, S. I., B. R. Ray, and N. C. Karmakar, "RFID localization in construction with IoT and security integration," *Automation in Construction*, Vol. 159, 105249, 2024.

[4] Parthiban, P., "Embeddable miniature UHF RFID near-field antenna for healthcare applications," *Progress In Electromagnetics Research M*, Vol. 87, 199–207, 2019.

[5] Wang, Y., "Leveraging and refining image recognition technology for intelligent logistics sorting systems," *Traitement du Signal*, Vol. 40, No. 3, 1235–1242, 2023.

[6] Luo, Y., M. R. Abidian, J.-H. Ahn, D. Akinwande, A. M. Andrews, M. Antonietti, Z. Bao, M. Berggren, C. A. Berkey, C. J. Bettinger, *et al.*, "Technology roadmap for flexible sensors," *ACS Nano*, Vol. 17, No. 6, 5211–5295, 2023.

[7] Musa, A. and A.-A. A. Dabo, "A review of RFID in supply chain management: 2000–2015," *Global Journal of Flexible Systems Management*, Vol. 17, No. 2, 189–228, 2016.

[8] Roggeveen, A. L. and R. Sethuraman, "Customer-interfacing retail technologies in 2020 & beyond: An integrative framework and research directions," *Journal of Retailing*, Vol. 96, No. 3, 299–309, 2020.

[9] Liu, X., J. Shannon, H. Voun, M. Truijens, H.-L. Chi, and X. Wang, "Spatial and temporal analysis on the distribution of active radio-frequency identification (RFID) tracking accuracy with the kriging method," *Sensors*, Vol. 14, No. 11, 20 451–20 467, 2014.

[10] Wang, S., Z. Liu, Y. Zhang, and Y. Li, "Active-passive reconfigurable antenna covering 70–7200 MHz bandwidth," *IEEE Transactions on Antennas and Propagation*, Vol. 72, No. 9, 7323–7328, 2024.

[11] Ferdous, R. M., A. W. Reza, and M. F. Siddiqui, "Renewable energy harvesting for wireless sensors using passive RFID tag technology: A review," *Renewable and Sustainable Energy Reviews*, Vol. 58, 1114–1128, 2016.

[12] Zhu, L. and T.-S. P. Yum, "Optimal framed aloha based anticollision algorithms for RFID systems," *IEEE Transactions on Communications*, Vol. 58, No. 12, 3583–3592, 2010.

[13] Klair, D. K., K.-W. Chin, and R. Raad, "A survey and tutorial of RFID anti-collision protocols," *IEEE Communications Surveys & Tutorials*, Vol. 12, No. 3, 400–421, 2010.

[14] Yaacob, M., N. Shafie, N. Mohamed, and A. Azizan, "Group collision tracking tree for passive multi-tags RFID systems," *International Journal of Integrated Engineering*, Vol. 16, No. 3, 257–272, 2024.

[15] Šolić, P., J. Radić, and N. Rožić, "Energy efficient tag estimation method for ALOHA-based RFID systems," *IEEE Sensors Journal*, Vol. 14, No. 10, 3637–3647, 2014.

[16] Thomas, A., M. M. Sylaja, and J. Kurian, "Leveraging time-domain signals for multi-tag classification in chipless RFID systems using classifier chains," *Progress In Electromagnetics Research C*, Vol. 156, 1–12, 2025.

[17] Görtschacher, L. and J. Grosinger, "Localization of signal pattern based UHF RFID sensor tags," *IEEE Microwave and Wireless Components Letters*, Vol. 29, No. 11, 753–756, 2019.

[18] Grosinger, J., L. Görtschacher, and W. Bösch, "Passive RFID sensor tag concept and prototype exploiting a full control of amplitude and phase of the tag signal," *IEEE Transactions on Microwave Theory and Techniques*, Vol. 64, No. 12, 4752–4762, 2016.

[19] Görtschacher, L. J. and J. Grosinger, "UHF RFID sensor system using tag signal patterns: Prototype system," *IEEE Antennas and Wireless Propagation Letters*, Vol. 18, No. 10, 2209–2213, 2019.

[20] Gao, Z., Y. Ma, K. Liu, X. Miao, and Y. Zhao, "An indoor multi-tag cooperative localization algorithm based on NMDS for RFID," *IEEE Sensors Journal*, Vol. 17, No. 7, 2120–2128, 2017.

[21] Rezaiesarlak, R. and M. Manteghi, "A space-time-frequency anticollision algorithm for identifying chipless RFID tags," *IEEE Transactions on Antennas and Propagation*, Vol. 62, No. 3, 1425–1432, 2014.

[22] Kheawprae, F., A. Boonpoonga, and D. Torrungrueng, "Complex natural resonance-based chipless RFID multi-tag detection using one-dimensional convolutional neural networks," *IEEE Access*, Vol. 11, 138 078–138 094, 2023.

[23] Wang, L., Z. Luo, R. Guo, and Y. Li, "A review of tags anticollision identification methods used in RFID technology," *Electronics*, Vol. 12, No. 17, 3644, 2023.

[24] Sarkar, S., "Three dual-band and dual-linearly polarized antenna configurations for UHF-RFID and WLAN applications," *IEEE Journal of Radio Frequency Identification*, Vol. 8, 571–579, 2024.

[25] Kumari, S., Y. K. Awasthi, and D. Bansal, "A miniaturized circularly polarized multiband antenna for Wi-MAX, C-band & X-band applications," *Progress In Electromagnetics Research C*, Vol. 125, 117–131, 2022.

[26] Yao, Y., Q. Ge, J. Yu, and X. Chen, "A novel antenna for uhf rfid near-field applications," *Electronics*, Vol. 10, No. 11, 1310, 2021.

[27] Barman, B., S. Bhaskar, and A. K. Singh, "Dual-band UHF RFID tag antenna using two eccentric circular rings," *Progress In Electromagnetics Research M*, Vol. 71, 127–136, 2018.

[28] Jin, K., Z. Geng, J. Zheng, Y. Liu, E. Zhang, Y. Yang, and X. He, "Analysis of dual-port reader antenna for UHF RFID near-field applications," *Progress In Electromagnetics Research M*, Vol. 72, 31–40, 2018.

[29] Gu, X. and W. Geyi, "Design of a near-field RFID antenna array in metal cabinet environment," *IEEE Antennas and Wireless Propagation Letters*, Vol. 18, No. 1, 79–83, 2019.

[30] Hester, J. G. D. and M. M. Tentzeris, "Inkjet-printed flexible mm-Wave Van-Atta reflectarrays: A solution for ultralong-range dense multitag and multisensing chipless RFID implementations for IoT smart skins," *IEEE Transactions on Microwave Theory and Techniques*, Vol. 64, No. 12, 4763–4773, 2016.

[31] Lai, F.-P. and Y.-S. Chen, "A broadband dual-polarized antenna with pattern reconfigurability for multi-tag detection in chipless RFID," *IEEE Transactions on Antennas and Propagation*, Vol. 73, No. 8, 6008–6013, 2025.

[32] Deng, W., Z. Li, Y. Xia, K. Wang, and W. Pei, "A widely linear MMSE anti-collision method for multi-antenna RFID readers," *IEEE Communications Letters*, Vol. 23, No. 4, 644–647, 2019.

[33] Dodds, L., I. Perper, A. Eid, and F. Adib, "A handheld fine-grained RFID localization system with complex-controlled polarization," in *Proceedings of the 29th Annual International Conference on Mobile Computing and Networking*, Vol. 7, 1–15, Madrid, Spain, Oct. 2023.

[34] Valagiannopoulos, C., "High selectivity and controllability of a parallel-plate component with a filled rectangular ridge," *Progress In Electromagnetics Research*, Vol. 119, 497–511, 2011.

[35] Monticone, F., C. Argyropoulos, and A. Alù, "Multilayered plasmonic covers for comblike scattering response and optical tagging," *Physical Review Letters*, Vol. 110, No. 11, 113901, 2013.

[36] Valagiannopoulos, C., "Effect of cylindrical scatterer with arbitrary curvature on the features of a metamaterial slab antenna," *Progress In Electromagnetics Research*, Vol. 71, 59–83, 2007.

[37] Rakibet, O. O., C. V. Rumens, J. C. Batchelor, and S. J. Holder, "Epidermal passive RFID strain sensor for assisted technologies," *IEEE Antennas and Wireless Propagation Letters*, Vol. 13, 814–817, 2014.

[38] Nan, X., Q. Jia, F. Lv, X. Wang, G. Wu, Y. Zhao, B. Qin, J. Hao, X. Cao, S. Mei, *et al.*, "A review of research on RF MEMS for metaverse interactions," *Journal of Micromechanics and Microengineering*, Vol. 34, No. 8, 083003, 2024.

[39] Wu, J., X. Cui, and Y. Xu, "A novel RFID-based sensing method for low-cost bolt loosening monitoring," *Sensors*, Vol. 16, No. 2, 168, 2016.

[40] Song, Z., B. Rahmadya, R. Sun, and S. Takeda, "An RFID-based wireless vibration and physical-shock sensing system using edge processing," *IEEE Sensors Journal*, Vol. 22, No. 20, 20 010–20 018, 2022.

[41] Liu, G., Q.-A. Wang, G. Jiao, P. Dang, G. Nie, Z. Liu, and J. Sun, "Review of wireless RFID strain sensing technology in structural health monitoring," *Sensors*, Vol. 23, No. 15, 6925, 2023.

[42] Medeiros, C. R., J. R. Costa, and C. A. Fernandes, "RFID reader antennas for tag detection in self-confined volumes at UHF," *IEEE Antennas and Propagation Magazine*, Vol. 53, No. 2, 39–50, 2011.

[43] Lorrain, P. and D. R. Corson, *Electromagnetic Fields and Waves*, W. H. Freeman and Company, 1970.

[44] Balanis, C. A., *Antenna Theory: Analysis and Design*, 4th ed., John Wiley & Sons, 2016.